Journal Pre-proofs

Effect of combined primary and secondary amine loadings on the adsorption mechanism of CO_2 and CH_4 in biogas

Basil Wadi, Ayub Golmakani, Vasilije Manovic, Seyed Ali Nabavi

PII: S1385-8947(21)01881-7
DOI: https://doi.org/10.1016/j.cej.2021.130294
Reference: CEJ 130294

To appear in: *Chemical Engineering Journal*

Received Date: 15 February 2021
Revised Date: 4 May 2021
Accepted Date: 7 May 2021

Please cite this article as: B. Wadi, A. Golmakani, V. Manovic, S. Ali Nabavi, Effect of combined primary and secondary amine loadings on the adsorption mechanism of CO_2 and CH_4 in biogas, *Chemical Engineering Journal* (2021), doi: https://doi.org/10.1016/j.cej.2021.130294

Chemical Engineering Journal, Volume 420, Pt. 3, September 2021, Article number 130294
DOI:10.1016/j.cej.2021.130294

Effect of combined primary and secondary amine loadings on the adsorption mechanism of CO_2 and CH_4 in biogas

Basil Wadi, Ayub Golmakani, Vasilije Manovic, Seyed Ali Nabavi*

Centre for Climate and Environmental Protection, Cranfield University, Bedford, Bedfordshire MK43 0AL, UK.

*Corresponding author: Seyed Ali Nabavi (s.nabavi@cranfield.ac.uk)

ABSTRACT

Biomethane, produced by biogas upgrading, is a promising energy source that can play a key role towards net-zero emissions targets. The incorporation of amine functionalities into adsorbents for biogas upgrading can facilitate the selective adsorption of CO_2, but their effect has not been comprehensively studied within the context of CH_4 mixtures. In this work, the effectiveness of amine functionalities in selectively separating CO_2 from biogas, is investigated. Primary, diamine, and triamine organo-silanes grafted at various loadings on SBA-15 were used to study the adsorption mechanisms associated with amine functionalities for CO_2:CH_4 gas mixtures. The successful incorporation of amines was confirmed with thermogravimetric analysis (TGA), Fourier Transform Infrared (FTIR), and elemental analysis (EA). The different amine reagents and loadings resulted in an alteration of adsorption mechanism that provided key information on the developing relationship between adsorption capacity, selectivity, and energy efficiency. Diamine with an amine loading of 2.5 mmol/g and a moderate silane coverage of 1.54 molecules/nm^2 was found to provide the best balance of an enhanced CO_2 adsorption capacity (1.12 mmol/g), a superior selectivity to densely grafted primary amines, and the lowest isosteric heat of adsorption of ~25 kJ/mol at 1.12 mmol/g compared to ~41 kJ/mol for primary and triamine materials. Amongst all the samples, a lower amine loading on the bare adsorbent enhanced CO_2 adsorption capacity and selectivity while minimising the heat duty associated with adsorbent regeneration. Moreover, under isothermal desorption conditions at 25 °C, some samples achieved working capacities comparable to higher amine loaded materials.

Keywords: Carbon capture; biogas upgrading; biomethane; amine grafting; SBA-15, functional adsorbents

1. Introduction

Atmospheric carbon dioxide (CO_2) concentrations reached a record high in 2020, with global averages reaching 414 ppm, being largely responsible for a global warming of ~ 1 °C[1]. To minimise severe consequences of climate change, it has become necessary to limit the extent of global warming to 1.5 °C from pre-industrial times by 2100, which would require meeting a net-zero emissions target by 2050[2,3].

Energy from fossil fuels continues to be the primary source of worldwide usage, but as a major contributor to greenhouse gases, has diverted research towards alternatives such as biogas[4]. Biogas, depending on the feedstock and upstream process, is a renewable energy source that can potentially be carbon neutral. Biogas is produced through anaerobic digestion, is primarily made up of CH_4 and CO_2, and is produced through processes that provide much lower lifecycle CO_2 footprints compared to fossil fuels[5,6]. This qualifies biogas as a feasible source of energy towards the UK's net-zero target. Moreover, upgrading biogas to biomethane for an increased calorific value while producing a high-purity CO_2 tail gas for storage can drive this initiative towards a negative-emissions energy source[7].

Amine scrubbing is a well-proven carbon capture technology that selectively absorbs CO_2. However, the energy demand for regeneration is high which leads to a large energy penalty[8,9]. An alternative to scrubbing that potentially imposes lower energy demand for regeneration is swing adsorption technology. Swing adsorption processes utilise solid adsorbents and come with the added benefit of flexibility in process arrangements allowing for a wide range of operating conditions for a diverse set of applications[10–12]. The favourable characteristics of amine scrubbing and swing adsorption can be combined through amine functionalisation of a variety of sorbent materials, although each material presents its own challenges and sensitivity to moisture, some examples include activated carbon[13] (AC), zeolites[14], mesoporous silica[15], and polymers[16,17]. The incorporation of amines into solid adsorbents can be carried out in a variety of methods, including grafting, impregnation, or in-situ doping, with various studies aiming to maximise the capacity of adsorbents through amine functionalisation utilising a wet-impregnation method on mesoporous silica such as MCM-41. This material has a high pore volume and can load up to 70 wt.% of polyethyleneimine (PEI) or tetraethylenepentamine (TEPA), with an optimal value of 50%-60% to minimise diffusional resistance[18–20]. Amine impregnation has been shown to enhance capacity and selectivity at low pressures, and due to the dominating effects of chemisorption at low CO_2 partial pressures, has been investigated for applications in flue gas treatment[21–23]. However, as the amine loading increases the required regeneration

temperature, the cyclability of these adsorbents is limited due to leaching. This is primarily caused by the absence of bonds between amine groups and the adsorbent surface[22,24,25]. In comparison, grafted amino organosilanes on mesoporous silicas form a covalent bond with the surface allowing for better cyclability. However, the maximum capacity is limited by the accessible surface silanols for amino-silane bond formations[26,27]. Whether by impregnation[18,19,28] or grafting[25,28–31] , many studies target high amine coverage to maximise adsorption capacity. These studies are mainly applied for post-combustion conditions, where the performance under CO_2/N_2 gas mixtures or in the presence of typical flue gas components is explored[22,23,30,32]. Hiyoshi et al.[24] studied SBA-15 with a range of surface functionalities on the adsorption of CO_2 in CO_2/N_2 mixtures. However, they focused on adsorption temperatures of 60°C and limited the CO_2 pressure to 15 kPa, conditions specific to flue gas. Alkhabbaz et al.[33] used calorimetry to understand the entropic and enthalpic contributions to the heats of adsorption of SBA-15 functionalised with 3-aminopropyltrimethoxysilane (APS) and several secondary amine structures. They deduced the importance of entropic factors in adsorbent CO_2 capture efficiency and showed the superiority of primary amines compared to secondary amines in achieving high CO_2 uptakes at ultra-low pressures, up to 10 kPa. Overall, there is a limited number of studies with respect to CO_2 adsorption efficiency ascribed to different amine functionalities and surface loadings in CO_2/CH_4 mixtures.

Mafra et al.[34,35] and Garcia et al.[28] both demonstrated the enhanced selectivity of CO_2 to CH_4 in amine-grafted SBA-15 at maximum grafting loadings. However, cyclic studies of SBA-15 functionalised with a high level of amines showed a lower working capacity for all amine types compared to raw SBA-15, at desorption conditions of 100 kPa and 10 kPa at 25 °C[35]. Similarly, in a cyclic stability study of triamine-functionalised SBA-15 in dry conditions, Belmabkhout et al.[32] reported a 67% loss in capacity under atmospheric desorption and a 20% loss under vacuum desorption at 25 °C. Although underperforming in dry conditions, in the same study they demonstrated the superior performance and cyclability of triamine-grafted MCM-41 at 7.5% relative humidity compared to zeolite 13x and Darco-AC commercial adsorbents. Belmabkhout et al.[15,36] also showed that at ambient temperatures, CH_4 interacts to a higher degree with functionalised and raw MCM-41 compared to N_2. For a fully functionalised MCM-41 with triamine, they reported a molar selectivity of 28 for CO_2/CH_4 compared to 308 for CO_2/N_2 at 100 kPa CO_2 partial pressure. Xu et al.[37] studied the adsorption of CO_2, CH_4, and N_2 mixtures on a monoethanolamine-modified β-zeolite from 5% to 60% functionalisation. They showed that at functionalities above 15%, selectivity is enhanced and a lower

uptake of all components including CO_2 is observed. The adsorbent's specific surface area reaches 17 m^2/g at this degree of amine functionalisation, which makes it difficult to determine the principal causes of the change in adsorption behaviour. This rationalises the need to utilise mesoporous media at low coverage to scrutinise the adsorbate-amine interactions to a greater degree. The lower coverage can provide essential information on the inter- and intra-molecular interactions at play while isolating them from diffusional limitations due to high loadings. The changes in inter- and intra-molecular interactions were analysed by Yoo et al.[38] through the heat of adsorption of mono-, di-, tri- and tetra-amines. They found that in certain cases, surface hydroxyl groups can interact with nearby amines to facilitate the chemisorption of CO_2. Their findings highlighted the potential utilisation of low amine loadings for CO_2 sorption. Nonetheless, the study was limited to ultra-low coverage and was not extended towards the selectivity of gas mixtures.

Limitations in the isothermal cyclic utilisation of amine-functionalised adsorbents, and the concentration of most studies on maximum amine loadings, highlight the necessity to understand the developing relationship between the level of functionality and adsorbent performance for these materials. In CO_2/CH_4 gas separations, further studies are required that scrutinise the developing relationship between amine loading, amine type, and the resulting separation efficiencies achievable.

In this work, a fundamental understanding of the change in adsorption mechanisms and separation efficiency with amine type and loading were studied, up to atmospheric pressure. This encompasses the initial pressure region in which the adsorption mechanisms of amine functionalised SBA-15 is undergoing a transition between chemisorption and physisorption. The effects of amine functionality on the adsorption of CO_2/CH_4 mixtures was thus investigated by grafting primary amine, di-amine and tri-amine organo-silanes on SBA-15 at varying amine loadings. The CO_2 and CH_4 capture capacity and selectivity of each amine type at different surface coverage was studied. This aided in the identification of amine-adsorbate interactions and elucidated important considerations in employing amine functionality for CO_2/CH_4 separations. Additionally, the isosteric heat of adsorption was calculated to understand the governing adsorption mechanisms as a function of amine type and amine loading. Finally, isothermal, and non-isothermal adsorption-desorption cycles were used to compare the implications of amine type and loading for low pressure adsorption, or temperature swing adsorption (TSA) applications.

2. Material and methods

2.1 Materials

As synthesised SBA-15 mesoporous silica was purchased in powder form from XFNANO®. The chemical reagents (3-aminopropyl)triethoxysilane (APTES), 3-(2-aminoethylamino)propyltri-methoxysilane (AEAPT), 3-[2-(2-aminoethylamino) ethylamino]propyltrimethoxysilane (TAEPT), toluene (99.8%), and methanol (HPLC grade) were purchased from Sigma-Aldrich, UK. All gases were supplied by BOC, UK with a purity above 99.99% for nitrogen, carbon dioxide, and methane.

2.1 Material Synthesis

For each sample, 1 g of SBA-15 was dried at 110 °C under vacuum (40 mbar) for 1 h to remove moisture and ensure minimal polymerisation of silane branches during grafting[26,34]. Once cooled, the system was purged with nitrogen, prepared for inert reflux, and 80 mL of toluene was introduced into the flask containing the SBA-15 powder. Subsequently, a given amount of amino organosilane was added as per **Table 1** (0.1-2 cm^3 of amine per gram of SBA-15) and the mixture was heated to 70°C for 18 h under reflux. The grafted SBA-15 was then filtered under vacuum suction and washed with an abundance of toluene and methanol. It is reported that drying of the sample in air can result in the oxidation of amino groups at elevated temperatures[39]. Therefore, the powder was left to dry in air for 24 h at room temperature. Each sample is designated as *S-x-y*, with *x* representing the amine type and *y* the amine loading.

2.3 Characterisation methods

2.3.1 Estimation of amine content

The quantity of amine grafted on each sample was estimated by thermogravimetric analysis (TGA 8000, PerkinElmer) and C and N elemental analysis (vario EL III, Elementar). The TGA measurement was carried out with a sample weight of 8-10 mg, under nitrogen flow from 30 °C to 800 °C at a rate of 20 °C /min, with a 10 min hold at 120 °C under nitrogen flow and a 5 min hold at 800 °C under air flow. Elemental analysis (EA) for C and N quantity was measured by a thermal conductivity detector through thermal combustion analysis.

2.3.2 Fourier Transform Infrared (FTIR) spectroscopy

FTIR spectra of samples over the range of 1000 - 3800 cm^{-1} were measured using a Shimadzu Attenuated Total Reflection (ATR) spectrometer to confirm the successful grafting of the amine branches and assess the gradual increase of functional moieties across all samples. Each sample was scanned 20 times at a resolution of 4 cm^{-1}.

2.3.3 Pore structure analysis

The structural properties were calculated from nitrogen adsorption isotherms at -196 °C using a 3P Meso 222 sorption analyser (3P Instruments). For each test, 0.2-0.3 g of sample was degassed at 90 °C for up to 2 h under vacuum. The specific surface area was calculated by the Brunauer-Emmett-Teller (BET) method in the relative pressure of 0.05 to 0.2[40]. The pore volume was calculated from the volume of adsorbed nitrogen at $p/p^o = 0.95$ using the Barrett-Joyner-Halenda (BJH) method[41]. The pore size distribution (PSD) was determined by the Broekhoff-de Boer (BdB) method simplified using the Frenkel-Halsey-Hill (FHH) approximation denoted as BdB-FHH[42]. Specific surface area, pore volume, and average pore size of samples are summarised in **Table 1**.

2.3.4 Volumetric gas adsorption measurement

CO_2 and CH_4 isotherms were measured using the 3P Instrument's sorption analyser. For each test, 0.25-0.3 g of sample was degassed under the same procedure previously described for nitrogen physisorption analysis. The adsorption temperature was maintained at 25, or 40 °C by submerging the sample tube in an anti-freeze liquid bath (3P Instruments). All measurements were taken up to 100 kPa.

The ideal gas adsorption theory (IAST) [43] method was employed to estimate the adsorption selectivity. It is important to note that the use of IAST is subject to certain limitations when applied to systems exhibiting energetic surface heterogeneity, or when one component adsorbs substantially more than the other [44,45]. Depending on the degree of functionalisation of the samples, surface heterogeneity may exist, especially at very low CO_2 pressures. This is due to unreacted amine moieties, chemisorption sites, or chemisorbed species distributed across the surface. Considering these limitations, this model is used as a comparative tool of the various functionalised samples relative to each other, providing insight on the different influences on CO_2/CH_4 selectivity, particularly concentrating at CO_2 partial pressures > 40 kPa, when chemisorption is no longer the principle adsorption mechanism.

The IAST selectivity ($\hat{S}$) was calculated using Eq (1):

$$\hat{S} = \frac{q_i/P_i}{q_j/P_j} \quad (1)$$

where q (mmol/g) and P (kPa) are equilibrium adsorption capacity and partial pressure of the gas species, respectively.

2.3.5 Gravimetric gas adsorption measurement

Gravimetric CO_2 adsorption and desorption for chosen samples were measured by TGA (TGA 8000, Perkin Elmer). A sample of 8-12 mg was degassed under a nitrogen flow of 60 mL/min at 110 °C for 30 min to ensure moisture is stripped away. The sample temperature was then stabilised at 25 °C and exposed to a flow of 60 mL/min of CO_2 for 25 min. The gas was then switched to nitrogen at 60 mL/min, and the temperature was kept at 25 °C for 30 min or increased at a rate of 15 °C/min to 40 °C and was maintained at 40 °C for 30 min.

3. Results and discussion

3.1. Surface analysis

Nitrogen adsorption-desorption isotherms of samples at -196 °C are given in Figure 1. All samples exhibited a type IV isotherm with an H1 type hysteresis loop, indicating a narrow distribution of uniform mesopores, a typical feature of SBA-15[46]. The introduction of amino organosilanes led to a reduction in adsorbent pore volume and specific surface area as the amine loading increases. In agreement with previous studies[22,47], the effect of grafted amine loading on the pore volume and specific surface area is more pronounced as the amine moieties per organosilane branch increase in number, with TAEPT having the most considerable effect at lower silane loadings followed by AEAPT and APTES. In the case of AEAPT (diamine), 22% more nitrogen loading was achieved at a comparable surface area of 308 and 317 m^2/g and pore volume of 0.78 and 0.81 cm^3/g for APTES and AEAPT, respectively. This is similarly seen with TAEPT, showing a 38% increase in nitrogen loading at a comparable surface area of 308 and 333 m^2/g and pore volume of 0.78 and 0.87 cm^3/g for APTES and TAEPT, respectively. Additionally, the affinity of each organosilane towards the formation of surface bonds varied based on the reagent used. Surface grafting occurred more readily at lower reagent volumes of 0.45 mL in the order of APTES >AEAPT>TAEPT, inversely proportional to the molecular length of each reagent.

The change in the pore size distribution with an increasing amount of grafted functional groups was calculated from the N_2 isotherms up to P/Po=0.85, which marks the final saturation plateau, and presented in **Figure S1** in the Supplementary Information[35,40,48,49]. It demonstrates the likely heterogeneous distribution of silane molecules within the pores of SBA-15, and clustering of amines or single isolated amines may both be present and should be considered when analysing the amine dependent CO_2 adsorption behaviour. The peak pore size for all functionalised samples was estimated from the nitrogen desorption branch showing a starting maximum pore diameter for raw SBA-15 of 7 nm.

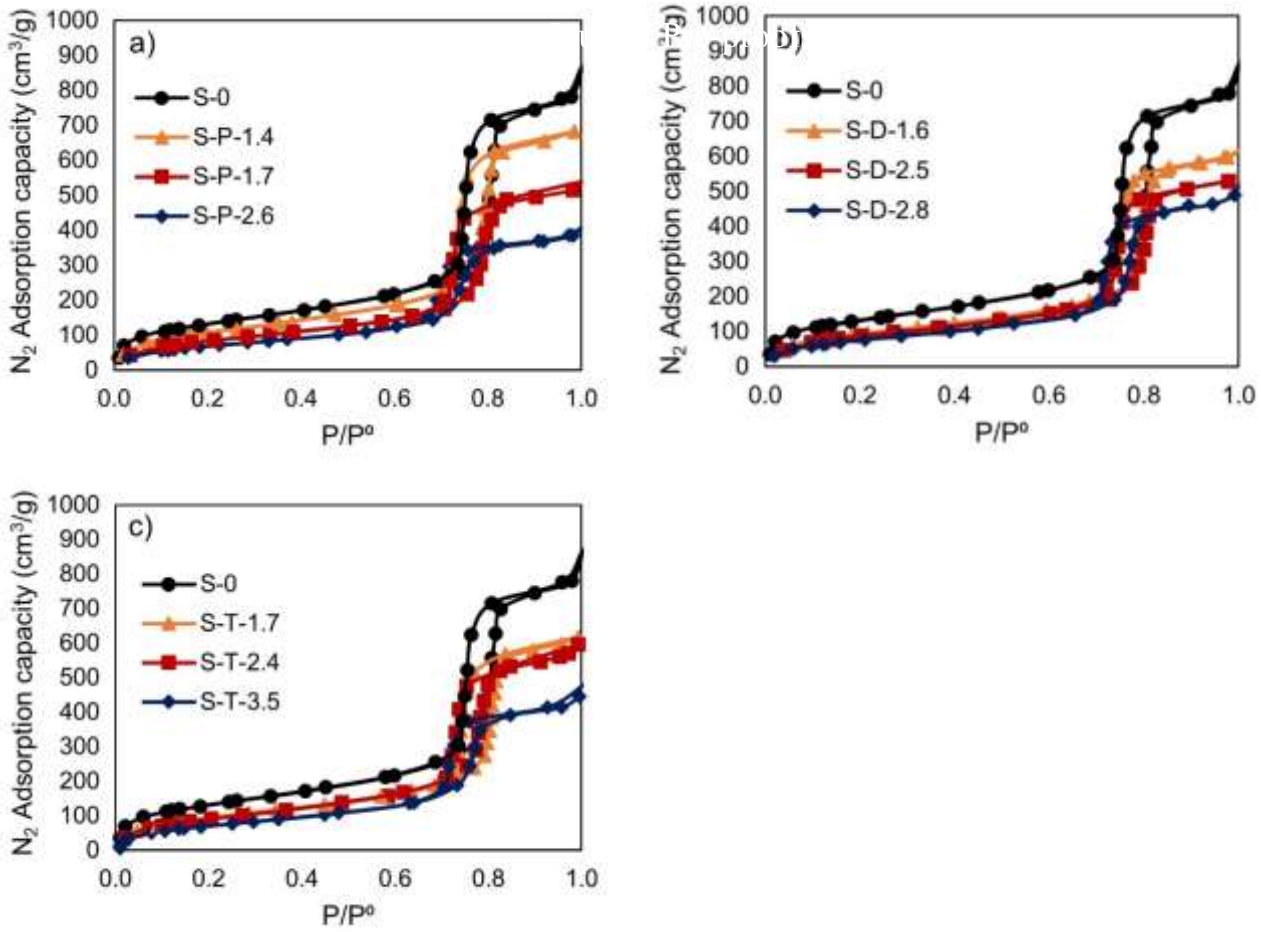

Figure 1. Nitrogen adsorption-desorption isotherms at -196°C for functionalised samples with different amine loadings of (a) APTES, (b) AEAPT, and (c) TAEPTs, in comparison with raw SBA-15.

Table 1. Physical and chemical properties of raw and functionalised SBA-15

				Amine loading (mmol/g)							
Sample	Reag-ent type	Reagent quantity (mL)	Amine type(S)	TGA – Tridentate/ Biden-OH*	TGA-Bidentate +	Elemental Analysis	Silane loading§	Silane Molecule/nm^{2} ‡	S_{BET} (m^2/g)	Vp (cm^3/g)	Dp (nm)
S-0	-		-	-	-	-	-	-	490	1.20	7.0
S-P-1.4	APTES	0.45	Primary	1.49	0.99	1.46	1.46	1.79	406	1.04	6.4
S-P-1.7	APTES	1.00	Primary	1.78	1.19	1.71	1.71	2.10	308	0.78	6.3
S-P-2.6	APTES	2.00	Primary	2.42	1.62	2.60	2.60	3.19	267	0.63	5.7
S-D-1.6	AEAPT	0.25	Primary Secondary	1.84	1.6	1.59	0.79	0.98	340	0.89	6.5
S-D-2.5	AEAPT	0.35	Primary/ Secondary	2.40	2.09	2.47	1.23	1.54	317	0.81	6.3

S-D-2.8	AEAPT	0.45	Primary/ Secondary	2.95	2.57	2.78	1.39	1.71	288	0.74	6.2
S-T-1.7	TAEPT	0.19	Primary/ 2 Secondary	2.09	1.89	1.70	0.56	0.70	352	0.92	6.8
S-T-2.4	TAEPT	0.23	Primary/ 2 Secondary	2.61	2.36	2.40	0.78	0.98	333	0.87	6.4
S-T-3.5	TAEPT	0.45	Primary/ 2 Secondary	3.90	3.53	3.52	1.17	1.44	274	0.66	6.3

* Estimate of amine loading from TGA data for tridentate-type bonding with the adsorbent surface or bidentate with an -OH side chain.
+ Estimate of amine loading from TGA data for bidentate-type bonding with the adsorbent surface with a methyl/ethyl branch remaining on the unsubstituted portion of the amino organosilane.
§ Silane loading calculated from the elemental analysis of each sample.
‡ Calculated amine surface coverage from the effective surface area of raw SBA-15 sample S-0 and the total measured amine loading in mmol/g.

3.1.2. Chemical properties

The measured infrared (IR) spectra of the functionalised samples (**Figure 2a**) confirm the successful grafting of the amino organosilanes on the surface of SBA-15. There is an increase in peak intensity at 1045 cm^{-1} coinciding with Si-O-Si bond vibrations within the range of 1130 – 1000 cm^{-1}. According to **Figure 2b**, the samples with the lowest loadings exhibit shallow peaks due to the small percentage of organics grafted (7%-10%). Nonetheless, there are clear peaks for NH_2 bending vibrations at around 1641 cm^{-1} for all primary amines. This is accompanied by the broad, yet weak band at 1566 cm^{-1} for organic silica containing a primary amine moiety. The presence of secondary amine moieties is more difficult to distinguish, but a magnification of the relevant IR regions associated with APTES, AEAPT, and TAEPT is provided in **Figure S2** in the Supplementary Information.

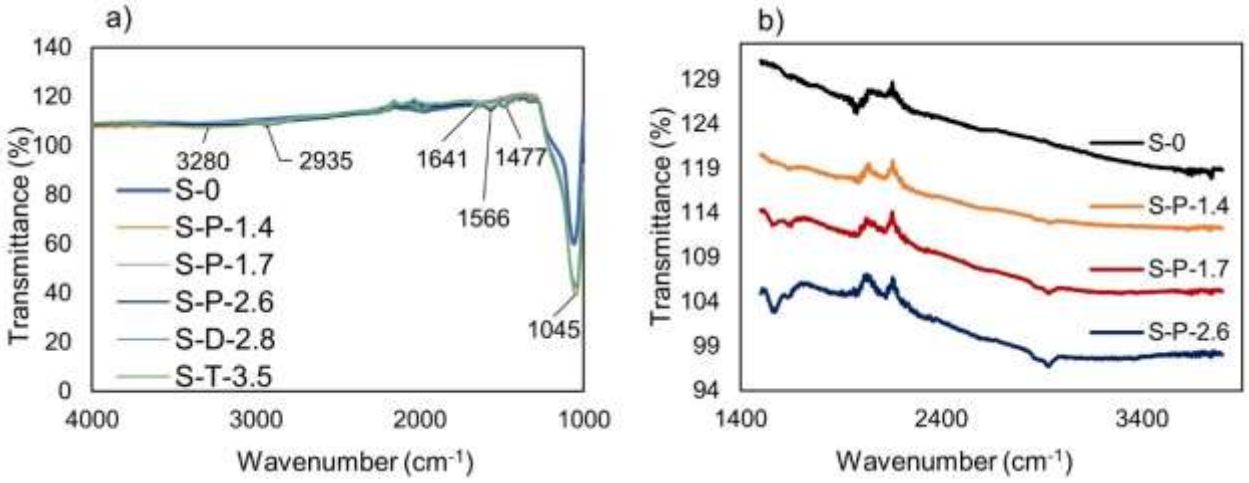

Figure 2. IR spectra for (a) selected functionalised samples and (b) primary amine-functionalised samples offset and magnified from 1500 to 3500 cm^{-1}, compared to raw SBA-15.

TGA results presented in **Figure S3** provide the total mass of grafted organic content. However, to accurately estimate the amine loading by TGA, an understanding of the bond type formed with the surface silanols is required. The possible variation in amine loading for different bonds between the organosilane and the surface can be seen in **Table 1**, as TGA – Bidentate and TGA-Tridentate. Bidentate refers to the formation of two bonds between the organosilane and the adsorbent surface while tridentate refers to grafting by forming three bonds. The R group in a bidentate surface bonding may exist as a methoxy in AEAPT and TAEPT, or ethoxy in APTES, or hydroxyl group for all amine reagents (**Figure 3**)[26,50]. It is important to note that the bidentate amine loading in **Table 1** only refers to the presence of methyl or ethyl on the R-group. On the other hand, the calculated amine loading, for a hydroxyl R-group, is considered as a tridentate bond.

For all amine types, the IR bands that coincide with the lateral methyl and ethyl branches, substituted during the grafting, are difficult to distinguish as they peak within 1075-1190 cm^{-1} and are masked by the sharper Si-O-R peak. The type of surface bonding was therefore estimated from a combined input of measured data, using both elemental analysis and TGA measurements. This was carried out using the total weight change attributed to organic content measured by TGA, and then correlated to the reported nitrogen content by EA. The weight measured by TGA can indicate different loadings of amines on the adsorbent' surface, and depends on the type of surface bond formed, which can be bidentate with a hydroxy, methoxy, or ethoxy side chain, or surface tridentate bonds[29,35]. The conversion of organic weight burnt off by TGA to amine loaded in mmol/g requires the molecular weight of the species bonded to the surface, which will vary depending on the type of bond formed between the amino organosilanes and the surface. Since the concentration of N and C from EA give an accurate total quantity of amines grafted, this can be related to the calculated amine loading from the TGA data, which will vary depending on different surface bonds and their respective molecular weight, giving an indication to the principal bond type formed. In this manner, the amine concentration measured from the Elemental Analysis can be correlated to the likelihood of a certain bond type. APTES data agrees with previous $^{1}H-^{29}Si$ heteronuclear correlation solid-state nuclear magnetic resonance (ssNMR) analysis by Mafra et al.[34], indicating a susceptibility for tridentate grafting with SBA-15 for this type of amine. In comparison, some of the diamine and triamine EA results can potentially indicate a higher quantity of bidentate bond types compared to primary amine-grafted samples. The method used limits definitive conclusions on the type of bonding due to possible silane polymerisation, shown to primarily result from the presence of moisture within the system[26,51]. Although the synthesis procedure was formulated to

ensure a moisture-free environment, there remains a possibility of polymerisation as suggested by previous research by Vrancken et al. of APTES grafted silica gel.

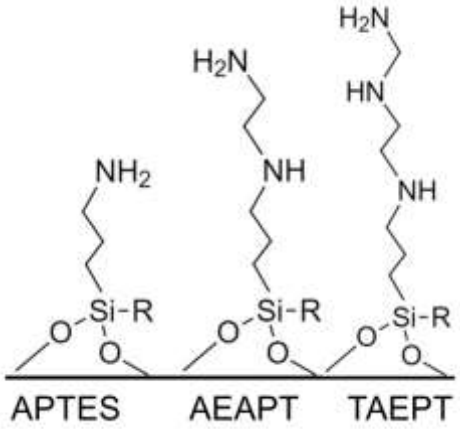

Figure 3. Silica surface grafted organo-silanes. R represents the methoxy or ethoxy or hydroxyl group in bidentate grafting. For tridentate grafting, all three silane branches are bonded to the surface of SBA-15 and R represents surface Si-O-Si bonds.

3.2 Adsorption mechanisms of CO_2 and CH_4

The measured CO_2 and CH_4 isotherms of the APTES, AEAPT, and TAEPT samples at 25°C and 40°C are provided in **Figures 4-6,** respectively. A summary of measured adsorption data, and estimated selectivity and heat of adsorption of samples are tabulated in **Table S1.** The measured CO_2 adsorption isotherms were fitted using the modified two-site Toth isotherm model, developed by Serna-Guerrero et al.[52], Eq. 2, and CH_4 adsorption isotherms were fitted by the Henry model, Eq. 3[53].

$$q = \left[\frac{n_s b_1 P}{\left(1 + (b_1 P)^{t_1}\right)^{1/t_1}}\right] + \left[\frac{n_{s2} b_2 P}{\left(1 + (b_2 P)^{t_2}\right)^{1/t_2}}\right] \quad (2)$$

$$q = KP \quad (3)$$

where n_s, b, and t are the Toth isotherm parameters with the *1* or *2* subscripts indicating the adsorption site. The variables $n_{\mu s}$, and b_μ represent the Sips isotherm constants, and n represents the Sips isotherm exponent. To understand the adsorption mechanisms as a function of amine loading, the isosteric heat of adsorption of each sample was calculated using the Clausius Clapeyron equation, Eq. 4 (**Figure 7**)

$$\ln \frac{P_2}{P_1} = \frac{-\Delta H_{Ads}}{R}\left(\frac{1}{T_2} - \frac{1}{T_1}\right) \quad (4)$$

where H_{Ads} is the isosteric heat of adsorption, T_1 and T_2 are the isotherm temperatures of the relative pressures of P_1 and P_2, and R is the universal gas constant.

For APTES samples (containing only a primary amine), an increase in amine loading from 1.4 N (S-P-1.4) to 1.7 N (S-P-1.7) caused a significant rise in the heat of adsorption (**Figure 7)**. However, the increase in heat of adsorption was moderate when amine loading was increased from 1.7 N to 2.6 N mmol/g (S-P-2.6). S-P-1.4, with the lowest loading, has the lowest heat of adsorption starting at ~ -50 kJ/mol then drops to -40 kJ/mol as q increases from 0.1 to 0.3 mmol/g. Compared to the raw sample S-0, there is an approximate increase of 20 kJ/mol in the heat of adsorption of S-P-1.4. Chemisorption can be characterised by heats of adsorption of > -40 kJ/mol with binding energies that separate chemisorption from physisorption at about 48 kJ/mol[54,55]. As a result, it can be concluded that S-P-1.4 shows a minimal enhancement of adsorption through chemisorption, but with a 62% increase in adsorption capacity compared to non-functionalised S-0 at 100 kPa and 25 °C (**Figure 4a**). In comparison, an increase in amine loading from 1.4 mmol/g (S-P-1.4) to 1.7 mmol/g (S-P-1.7) resulted in a 33% increase in adsorption capacity at 100 kPa but was accompanied by a considerable rise in the heat of adsorption (121 kJ/mol at 0.3 mmol/g). This is likely a result of the higher availability of adjacent amine sites in the S-P-1.7 sample, satisfying the 2:1 amine-to-CO_2 ratio expected for chemisorption to occur under dry conditions and the formation of carbamate or carbamic acid[56,57].

A further increase in amine loading from 1.7 mmol/g (S-P-1.7) to 2.6 mmol/g (S-P-2.6) did not have a significant effect on the heat of adsorption but enhanced the CO_2 capacity by 30% at 100 kPa (146 kJ/mol at 0.3 mmol/g). This may be a result of the initial fast reaction between CO_2 and the readily available amine sites, resulting in a strong interaction between adsorbate and amine, and a higher heat of adsorption at loadings below 0.4 mmol/g. This initial spike in adsorption is followed by a more uniform distribution of CO_2 on the remaining active sites in a manner comparable to S-P-1.7 and subject to similar interaction strengths.

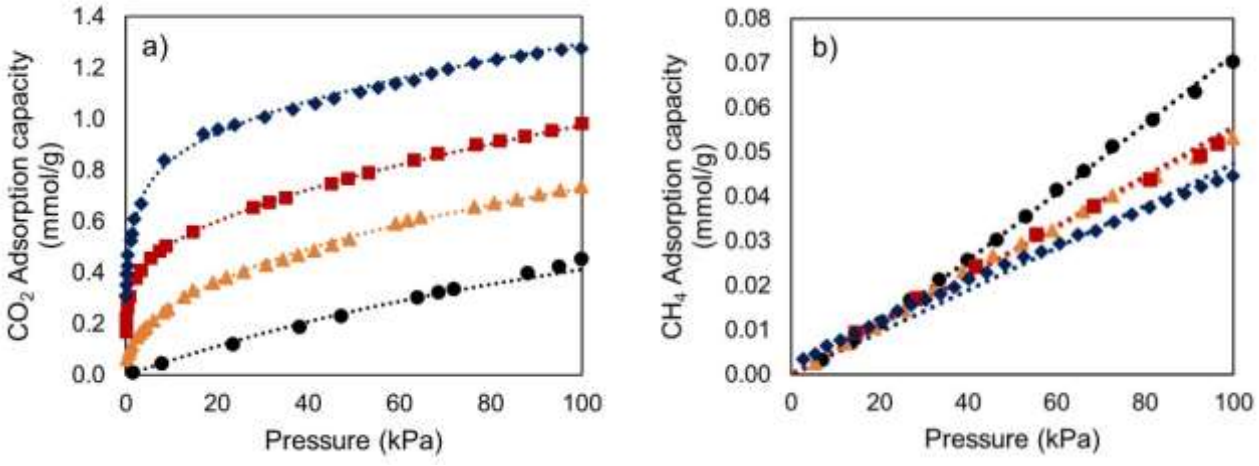

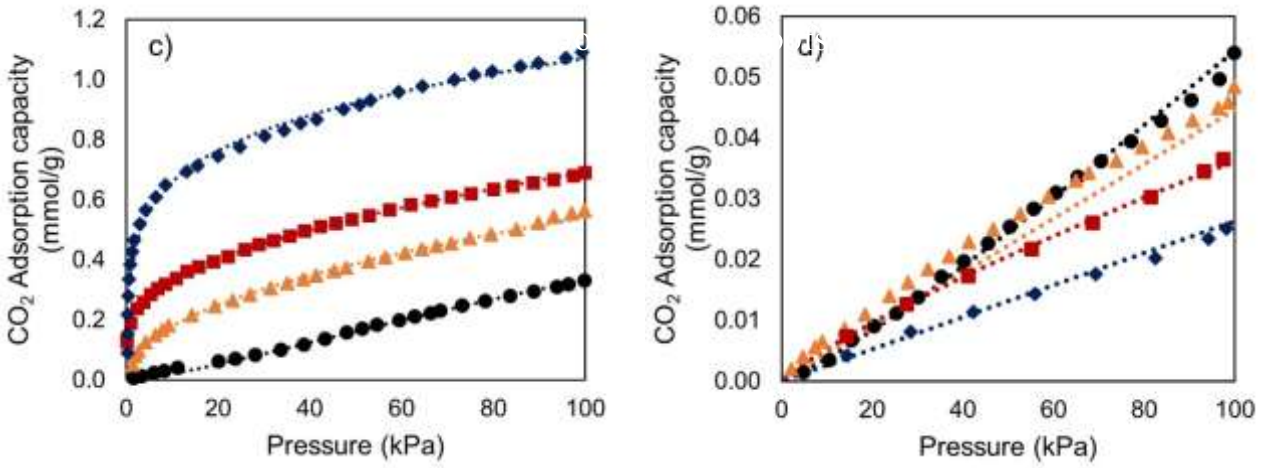

Figure 4. Adsorption isotherms of APTES grafted SBA-15 for (a) CO_2 at 25 °C and (b) CH_4 at 25 °C, (c) CO_2 at 40 °C and (d) CH_4 at 40 °C (●) S-0, (▲) S-P-1.4, (■) S-P-1.7, (◆) S-P-2.6. The dotted lines represent the model predictions.

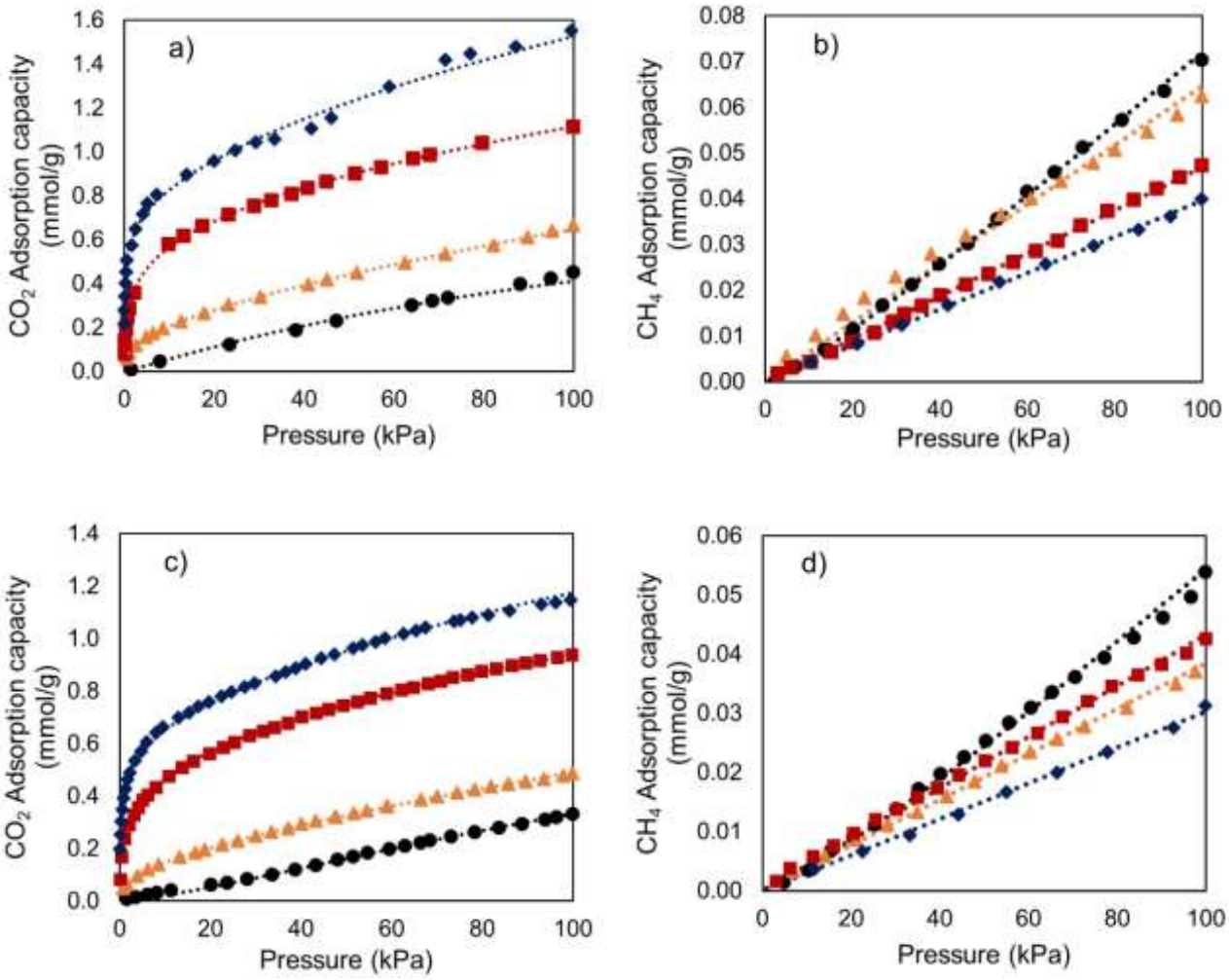

Figure 5. Adsorption isotherms of AEAPT grafted SBA-15 for (a) CO_2 at 25 °C and (b) CH_4 at 25 °C, (c) CO_2 at 40 °C and (d) CH_4 at 40 °C (●) S-0, (▲) S-D-1.6, (■) S-D-2.5, (◆) S-D-2.8. The dotted lines represent the model predictions.

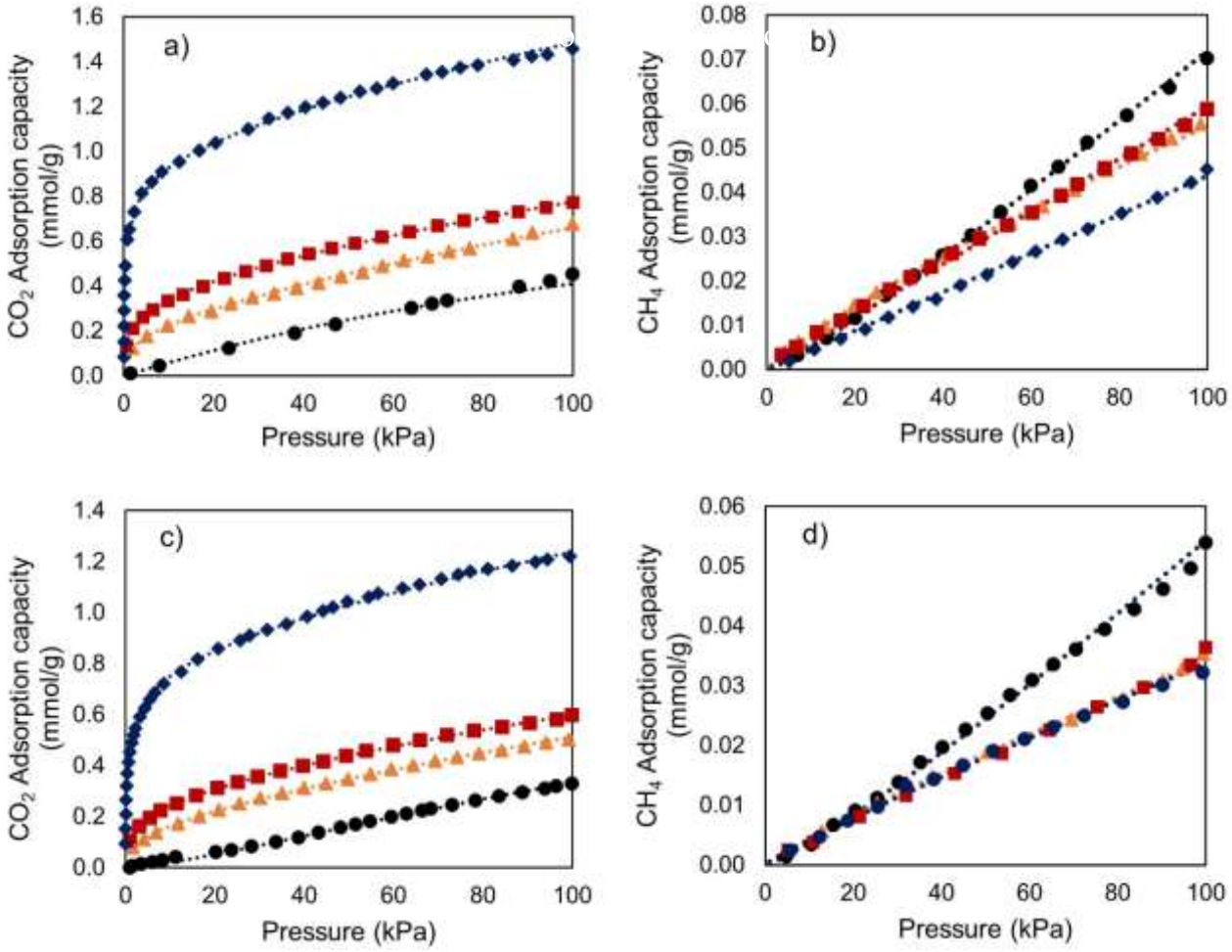

Figure 6. Adsorption isotherms of TAEPT grafted SBA-15 for (a) CO_2 at 25 °C and (b) CH_4 at 25 °C, (c) CO_2 at 40 °C and (d) CH_4 at 40 °C (●) S-0, (▲) S-T-1.7, (■) S-T-2.4, (◆) S-T-3.5. The dotted lines represent the model predictions.

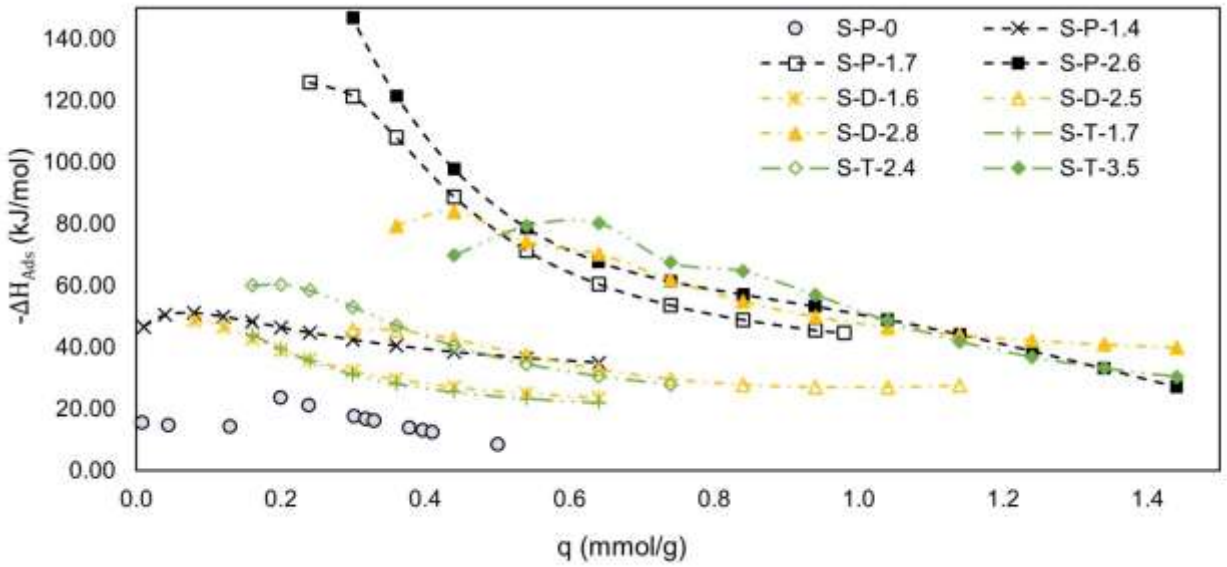

Figure 7. Isosteric heat of adsorption for raw SBA-15 and functionalised samples

For AEAPT samples (containing one primary and one secondary amine), an increase in amine loading from 1.6 (S-D-1.6) to 2.5 N mmol/g (S-D-2.5) caused a considerable enhancement in adsorption capacity from 0.3 to 0.6 mmol/g (**Figure 5a)**, while only a slight rise in heat of adsorption (~ 15 kJ/mol) was observed (**Figure 7**). This response is distinctive compared to the APTES samples since S-D-2.5 achieves an adsorption capacity across all pressures that exceeds S-P-1.7 but with a heat of adsorption closer to S-P-1.4 (60 to 25 kJ/mol). Similar performance has been previously reported for secondary amine containing amino organo-silanes and can be explained by the formation of lower stability carbamic acid, and the availability of two amine pairs along the same silane chain to satisfy the 2:1 requirement for the chemisorption of CO_2 while minimising the occupation of active sites for physisorption on the adsorbent surface[33,58].

For TAEPT samples (containing one primary and two secondary amines), a contrasting trend was observed with S-T-1.7, S-T-2.4, and S-T-3.5: they have higher nitrogen loadings than their diamine counterparts yet lead to a noticeably smaller enhancement in adsorption capacity at an equivalent $-\Delta H_{Ads}$ (**Figure 5a and c, Figure 6a and c, Figure 7**). A comparison of S-T-2.4, S-D-2.5, and S-P-2.6 highlights the effects of increasing amine moieties at similar amine loadings, and indicates that at this level of coverage, CO_2 uptake reaches 0.78 mmol/g, 1.12 mmol/g, and 1.29 mmol/g, respectively.

The sorbents with high loading of primary, diamine, and triamine agree with Zelenak et al.[58] work. Primary and diamine samples having similar heats of adsorption along a wider range of CO_2 loadings. In their work triamine grafted at 3.6 mmol/g presented an overall lower heat of adsorption than both primary and diamine. However, in their case the S_{BET} and pore volume was much smaller than presented samples in this study. For materials with lower loading, Yoo et al.[59] presented calorimetric data of diamine and triamine grafted at 0.85 mmol/g and 1.2 mmol/g of amine, showing similar heats of adsorption starting at 80 kJ/mol and following a decreasing profile similar to the one presented in **Figure 7.**

These results demonstrate that a higher amine efficiency is obtained from only primary amine-grafted samples compared to a mixture of secondary and primary amine moieties. Triamine, which contains two secondary amines per each primary amine, leads to a less efficient utilisation of amine moieties for chemisorption, even at low amine loadings. This has been attributed to steric hindrances that reduce the total number of accessible secondary amines[24,47]. There is also a limitation on the intramolecular interaction of adjacent amines, which hampers the realisation of a 2:1 stoichiometric ratio of amine to CO_2 for carbamate formation under dry conditions[56,60,61]. Additionally, recent studies by Cendak et al.[62] confirmed the

presence of isolated CO_2 species in APTES modified SBA-15 with controlled amine spacing creating isolated APTES branches. Their study combined with the higher amine efficiency observed by APTES in this work indicates that secondary amines may similarly enhance the adsorption of CO_2, evidenced by the low heat of adsorption observed in diamine and triamine.

For Chemisorption of CO_2 by diamine and triamine branches, there are many possible amine-amine and amine-adsorbent interactions, shown most recently through NMR spectroscopy by Szego et al.[63]. However, it has been reported by Hahn et al.[64] and Mafra et al.[34] that there is a tendency for a secondary amine to be protonated and stabilised by surface hydrogens (from hydroxyl groups), in place of chemisorbed CO_2 (as carbamate or carbamic acid), thus lowering the available amine sites for CO_2 adsorption. Additionally, triamine organosilanes have the longest molecular length, and Hahn et al.[64] and Zelenak et al.[58] proposed that a primary amine moiety and a secondary amine moiety can interact to adsorb CO_2 along one amine branch. This is more likely to occur in the absence of lateral amines and at low grafted amine coverage. This leaves the lower secondary amine unpaired, and prone to be stabilised by surface bonds, making it unavailable for CO_2 chemisorption at the pressures studied. Results here confirm hypothesis by Zelenak et al.[58], which attributes a smaller contribution from chemisorption as the molecular length of the organosilane increases, and a larger influence of physisorption in the adsorption of CO_2 as pressure increases.

Figures 4c, 5c, and 6c present the CO_2 adsorption isotherms of APTES, AEAPT, and TAEPT at 40 °C. Although amines primarily interact with CO_2 via chemisorption, a mechanism that is assisted by higher operating temperatures, a decrease in total capacity was observed as the adsorption temperature increased from 25 to 40 °C. This observation is in agreement with studies by Sayari and co-workers[52,60] on primary- and triamine-functionalised MCM-41 from 25 to 55 °C. Investigating the decrease in capacity observed for primary amine shows a 0.28 mmol/g decrease in S-P-1.7 compared to 0.19 and 0.21 mmol/g for S-P-1.4 and S-P-2.6, respectively. There is also a clear shift from a flatter slope in initial CO_2 uptake towards a much steeper rise as amine loading increases. The larger decrease in adsorption capacity by S-P-1.7 indicates the availability of more physisorption sites compared to S-P-2.6, due to the higher dependency of adsorption on temperature. Since S-P-1.4 did not demonstrate an equivalent decrease in capacity, these physisorption sites in S-P-1.7 are likely caused by polarised chemisorbed species acting as physisorption sites, as has been previously suggested by Mafra et al. [34,35] This may additionally be attributed to the distribution of active amine sites along the length of the adsorbent's cylindrical pores, a higher amine loading closer to the

adsorbent surface hinders the diffusion of CO_2 into the pores, leading to a larger drop in capacity at higher temperatures[65,66]. To further explore this hypothesis, adsorption data measured by TGA for CO_2, across the varying loadings of primary amine grafted SBA-15, is presented in **Figure S4.** There is initial faster adsorption by S-P-1.7, indicating more accessible amine sites for CO_2-amine interactions compared to S-P-1.4 and S-P-2.6. There may be additional factors involved, but results presented here show the larger role physisorption has in S-P-1.7 compared to S-P-2.6, and is supported by the similarities in the heat of adsorption for both samples at CO_2 loadings above 0.4 mmol/g, as presented in **Figure 7**.

In the case of AEAPT, from 25 to 40°C the adsorption capacity of both S-D-1.6 and S-D-2.5 at 100 kPa decreases by 0.17 mmol/g (26% and 16%, respectively). The largest drop in capacity of 0.40 mmol/g (a further 26%) is seen for S-D-2.8, the densest sample with the smallest pore volume (0.74 cm^3/g). Comparable to S-P-1.7 (V_p = 0.78 cm^3/g), this may be a consequence of diffusion effects from the longer AEAPT molecule, due to localised clustering of the organosilanes within the adsorbent pores. The CH_4 adsorption capacity and selectivity (separation factor) can highlight the effects of amine type and surface coverage on the performance of grafted adsorbents. It was found that in all samples, an increase in amine surface coverage caused a reduction in the total adsorbed CH_4, and the highest amine loading showed the largest decrease in CH_4 adsorption capacity. The decrease in adsorption capacity was dependent on the type of amine employed, with a minimum and maximum decrease (from raw SBA-15) of 11% for S-D-1.6, and 42% for S-D-2.8. The similarity in uptake can be attributed to the overall weak affinity of the adsorbent towards CH_4 molecules below 100 kPa. The individual contribution of porosity and intermolecular interactions can be scrutinised by correlating the available pore volume and silane surface coverage to changes in adsorbate uptake (**Figure S5**). It is important to note that at lower silane loadings the overall effect on CH_4 adsorption is weak, especially at 40 °C; this can potentially lead to similar CH_4 uptake amongst some samples such as AEAPT samples presented in **Figure 5d** for S-D-1.6 (silane loading of 0.79 mmol/g) and S-D-2.5 (silane loading of 1.23 mmol/g) at 40 °C. However, the evidently weak intermolecular forces at this temperature between diamine and CH_4 accentuate the different adsorption behaviour of each amine type, with APTES demonstrating a smaller variation in uptake at 25 °C instead of 40 °C (**Figure 4b and d**). For triamine at 40 °C, the extent of reduction in CH_4 adsorption was limited to a minimum; all three samples adsorbed almost the same quantity of CH_4 of ~0.033 mmol/g, a 38% decrease from S-0 (**Figure 6d**)**.**

At equivalent silane surface coverage, triamine and diamines exhibit a similar CH_4 uptake **(Figure S5b).** This is not the case for primary amine, as its shorter molecular length leads to a higher uptake at a similar level of molecules/nm^2. Investigating the effect of pore volume, as presented in **Figure S4a**, S-P-2.6 and S-T-3.5 with high amine functionalisation led to similar adsorption capacities, likely attributed to the pore blockage from the low pore volume of 0.63 and 0.66 cm^3/g, respectively. At moderate coverage, S-P-1.7 (V_p = 0.78 cm^3/g) achieved an uptake 18% higher than S-D-2.5 (V_p = 0.81 cm^3/g) and 3.7% lower than S-T-2.4 (V_p = 0.87 cm^3/g). The association of available effective surface area and CH_4 adsorption is especially pronounced in the higher coverage samples (S-P-2.6, S-D-2.8, and S-T-3.5) as can be seen in **Figure 4b, 5b, and 6b**, and in adsorption isotherms at 40°C for APTES and AEAPT (**Figure 4d and 5d**). It is not clear if electrostatic interactions between CH_4 and primary and secondary amines play a part in the change in CH_4 adsorption due to different amine coverage. Further experiments should be carried out at higher pressures to better understand the role of amine grafting in CH_4 adsorption mechanism, whether it is a result of electrostatic forces between the amine groups and CH_4, a decrease in pore volume and effective surface area, or a combination of both.

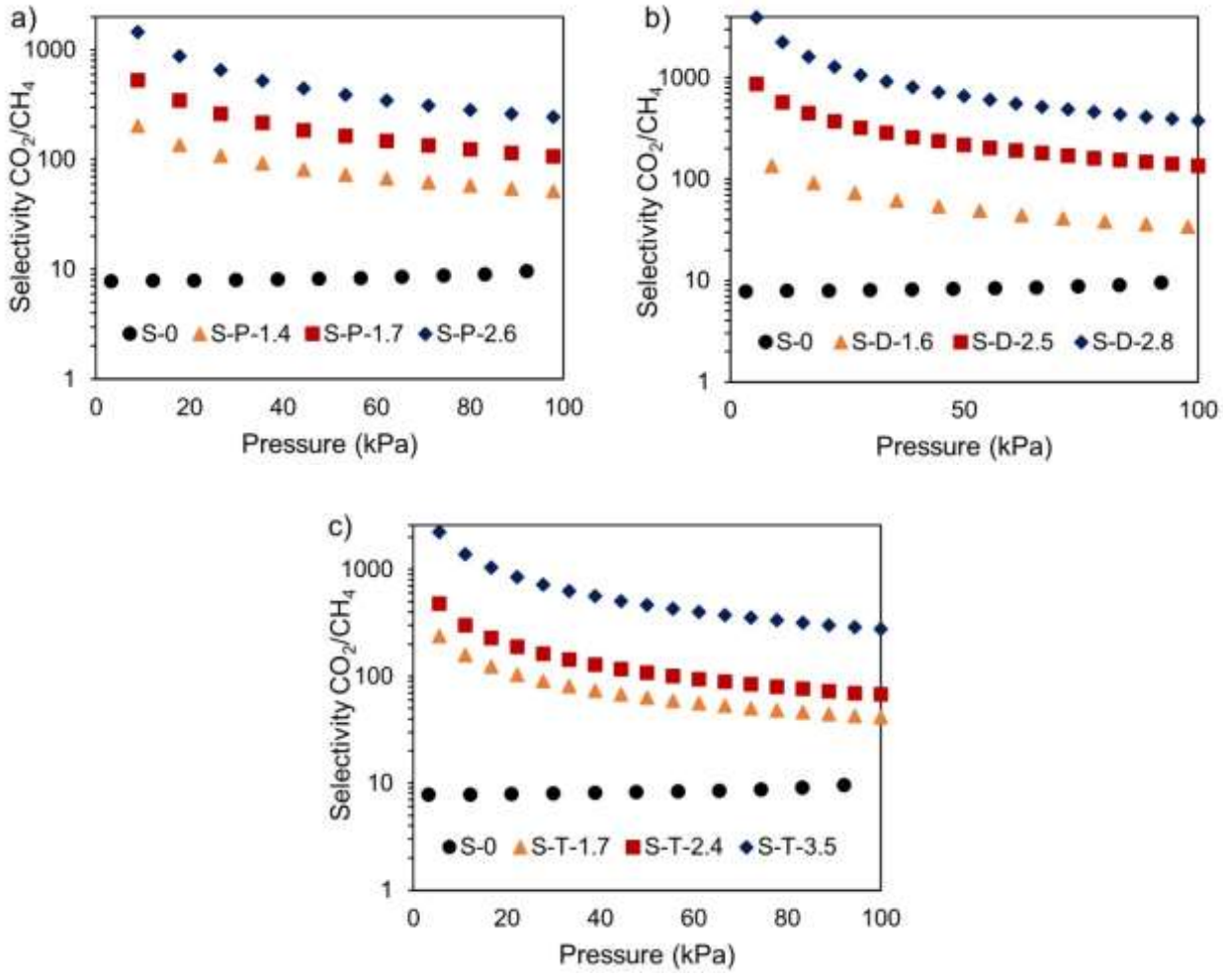

Figure 8. CO_2/CH_4 IAST selectivity (log scale) at 25 °C up to 100 kPa pressure of a 60:40 CH_4:CO_2 mixture for raw SBA-15 with (a) APTES, (b) AEAPT, and (c) TAEPT at different amine loadings.

Figure 8 presents the CO_2/CH_4 selectivity of all samples at 25 °C. All samples become more selective towards CO_2 as the amine quantity increases. At a CO_2 partial pressure of 40 kPa (**Figure 9**), the primary amine with the lowest loading (S-P-1.4) shows a higher selectivity (51) compared to S-D-1.6 (34) and S-T-1.7 (41), even though all have similar amine loadings. On the other hands, for the samples with the highest CO_2 uptake, S-P-2.6 had the lowest selectivity of 240, compared to 374 for S-D-2.5 and 276 for S-T-3.5.

Referring to **Figure 9**, there is a linear increase in selectivity as amine loading increases, which may indicate similar molecular interactions between CH_4 and the amine moieties. This interaction can be associated with a primary or secondary moiety, depending on the distribution of the organosilane branches and the accessibility of the CH_4 molecule to the amine moiety. This is seen by S-D-2.8, which is more linearly related to the APTES samples, indicating similar primary amine interactions. While in comparison, S-T-3.5 is more linearly related to the remaining AEAPT and TAEPT materials, indicating a combined contribution of primary and secondary amine interactions with CH_4, coupled with likely steric influences. Simultaneously, accessible amines act as active sites for CO_2 adsorption, through both chemisorption and physisorption interactions. Thus, the linear relationship can be attributed to the same accessible amine moieties, influencing both CO_2 and CH_4 adsorption, with a much stronger effect on the former adsorbate.

At a higher temperature of 40 °C (**Figures S6 and S7**), the selectivity follows a similar order, and referring to APTES and TAEPT functionalised samples with high CO_2 adsorption capacities, the selectivity of S-P-1.7, S-P-2.6 and S-T-3.5 increase by almost equivalent magnitudes. Comparatively, AEAPT functionalised samples both showed a decrease in the selectivity, especially in S-D-2.8. At this temperature, S-P-1.4, S-D-1.6, and S-T-1.7 all have very similar selectivity values ranging from 31 to 41. The effect of temperature on the selectivity of higher-loaded samples can be a result of the lower quantity of CO_2 physisorption active sites in S-P-2.6 and S-T-3.5, in these materials, the temperature increase has a smaller effect on CO_2 adsorption, indicating a lower quantity of CO_2 adsorption by Van der Waals forces.. Additionally, at both temperatures, the effect of molecular interactions between amines and the octupole moment of CH_4 should be considered. Low to moderate loadings of APTES may indicate a higher degree of CH_4 adsorbate-amine interactions

compared to AEAPT and TAEPT, even when pore volume contributions are considered, as discussed previously.

At very low CO_2 partial pressures, chemisorption is the dominant adsorption mechanism in all functionalised samples, but the selectivity remains a relevant parameter for the comparison of the extent of separation. At a pressure of 11 kPa of a 40:60 CO_2:CH_4 mixtures, the IAST selectivity of S-P-2.6, S-D-2.5, and S-T-3.5 are 1317, 2251, and 1390, respectively. The deviation in selectivity amongst these samples at this pressure follows the same trend as at 40 kPa CO_2 partial pressure, but with larger differences in selectivity that continue to rise as pressure decreases below 5 kPa, coinciding with the initial high CO_2 uptake via chemisorption.

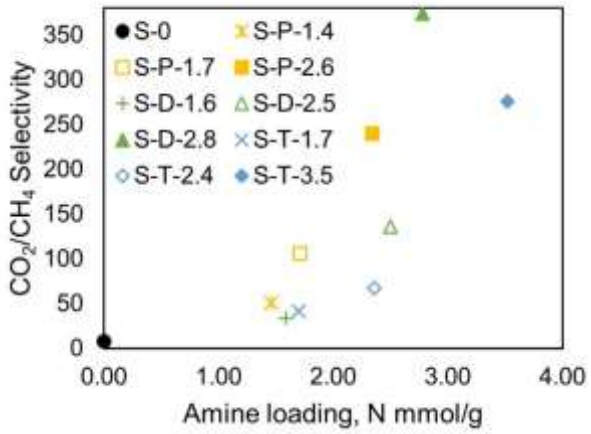

Figure 9. CO_2/CH_4 selectivity as a function of amine loading of functionalised SBA-15 at CO_2 partial pressure of 40 kPa and 25 °C

The CO_2/CH_4 adsorption characteristics of prepared samples in this work, in comparison with other adsorbents in literature are provided in **Table S2** (SI). The low CH_4 adsorption capacity and high CO_2/CH_4 selectivity of presented samples can be considered superior to most benchmark adsorbents, even at low amine loadings of 1.4-1.7 mmol/g. Calgon BPL and Norit C carbon-based adsorbents were shown to be limited to a selectivity of ~3, with CH_4 capacities > 0.45 mmol/g[67]. Zeolite 13x was shown to adsorb similar quantities of CH_4 to the carbon cased adsorbents (~ 0.5 mmol/g), but has a larger molar selectivity of 13-15 due to the higher CO_2 (4.5 mmol/g)[68,69]. MOFs, such as MIL-53 (Cr) and MOF-508b, have CH_4 capacities of 0.4-0.5 mmol/g, with CO_2 capacity of 1.2-1.6 mmol/g in equimolar CO_2/CH_4 breakthrough experiments at 100-200 kPa and 30°C[70,71]. A more recent study by Golmakani et al.[7] on novel polymeric adsorbents, showed slightly higher CH_4 adsorption of 0.12 mmol/g compared to the adsorbents presented here, with CO_2 adsorption capacity of 0.6 mmol/g. Higher CH_4 adsorption capacities result from the adsorbents presented

here compared to low-moderate amine grafted SBA-15, which in this study show significantly lower CH_4 adsorption of ~0.05 – 0.06 mmol/g, at CO_2 adsorption capacities that range from 0.68 to 1.11 mmol/g. However, it should be noted that the enhanced selectivity of amine functionalities imposes energy penalties of regeneration, which is what makes this study scrutinizing the correlation between amine loading and separation efficiency necessary to further advance the development of state-of-the-art adsorbents.

3.3. Isothermal versus non-isothermal operation

Isothermal and non-isothermal performance can provide valuable information on the regeneration efficiency for each amine type and surface loading. The presented data aims to support conclusions made from the calculated heat of adsorption, while comparing the efficacy of the prepared materials to desorb CO_2, either by temperature modulation or by CO_2 partial pressure modulation (using a purge gas). These results are the first step towards narrowing down the energy dependency of each amine type and loading for commercial pressure swing processes, following the pelletisation of the utilised SBA-15 powder. The desorbed quantity of CO_2 can confirm the conclusions made from the equilibrium adsorption data and the heats of adsorption. **Figure 10** presents the adsorption uptake per amine loading (molar quantity of adsorbed CO_2 per mmol of nitrogen per gram of adsorbent), under isothermal adsorption-desorption at 25 and 40 °C (**Figure 10a and c**), and non-isothermal conditions with adsorption carried out at 25 °C and desorption at 40 °C (**Figure 10b**), measured by TGA. S-P-2.6 has the highest adsorption efficiency as a function of amine quantity. However, referring to **Figure 11**, which summarises the molar fraction desorbed per molar fraction adsorbed (C_{Des}/C_{Ads}), it loses almost 46% of its adsorption capacity after the first cycle under atmospheric desorption at 25 °C. This can indicate that functionalisation to a maximum extent is not always beneficial at these operating conditions. This is highlighted by the isothermal cycle at 40 °C, in which desorbed quantities are equivalent to the 25 °C isothermal cycle for all samples, except S-P-1.4 and S-T-2.4. This loss of capacity makes S-P-1.4, S-P-1.7 and S-D-2.5 comparable alternatives under isothermal operating conditions; they provide a working capacity and amine efficiency equivalent to S-P-2.6 and S-D-2.8 while outperforming S-T-2.4 and S-T-3.5. Under a higher desorption temperature of 40 °C the samples with higher loading, specifically S-P-2.6, S-P-1.7 and S-D-2.8, achieve the highest adsorption per amine efficiency by a large margin. The difference between S-P-2.6 and S-P-1.7 is small, suggesting that amine efficiency does not increase proportionally with amine loaded, and moderate functionalities may provide better performance under cyclic low-temperature operation.

According to **Figure 4a**, under equilibrium adsorption at 100 kPa and 25°C, S-P-1.4 achieved a capture capacity of 0.74 mmol/g compared to 0.45 mmol/g for S-0. The increase in adsorption capacity is a result of the incorporation of amines which enhance adsorption of CO_2 primarily by chemisorption. However, in **Figure 11**, under isothermal desorption, the enhancement in capacity is still significant, as only a 0.15 mmol/g loss in capacity is measured at 25°C compared to the 0.29 mmol/g enhancement in total adsorption for S-P-1.4. This quality is shared by all the samples with a lower amine loading, demonstrating a lower heat of adsorption. The results from isothermal desorption at 25 °C under nitrogen flow support studies by Mafra et al.[34,35]. They concluded that under certain conditions less stable carbamic acid species are formed and stabilised by surface hydrogens. These formed entities are more readily desorbed under milder conditions. This may imply that a right balance of amine functionalisation for effective isothermal desorption and cage-like internal morphology for a pressure dependence of adsorption-desorption cycles would provide the ideal adsorbent formulations for PSA and pressure vacuum swing adsorption (PVSA) applications.

To further progress the work towards commercial pressure swing application, the future research should focus on the functionalisation of palletised SBA-15 based on the outcomes of this work, in order to enable fixed bed breakthrough measurement using binary gas mixtures, and under isothermal/non-isothermal desorption conditions.

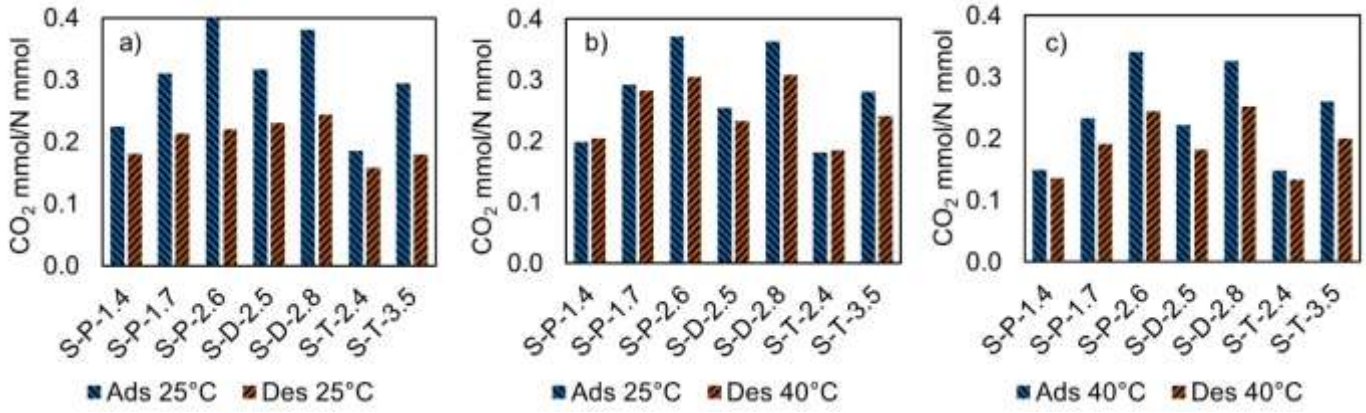

Figure 10. CO_2 molar capacity per amine loaded at (a) isothermal adsorption-desorption cycle of 25 °C, (b) non-isothermal adsorption-desorption from 25 °C to 40 °C, and (c) isothermal adsorption-desorption cycle of 40 °C.

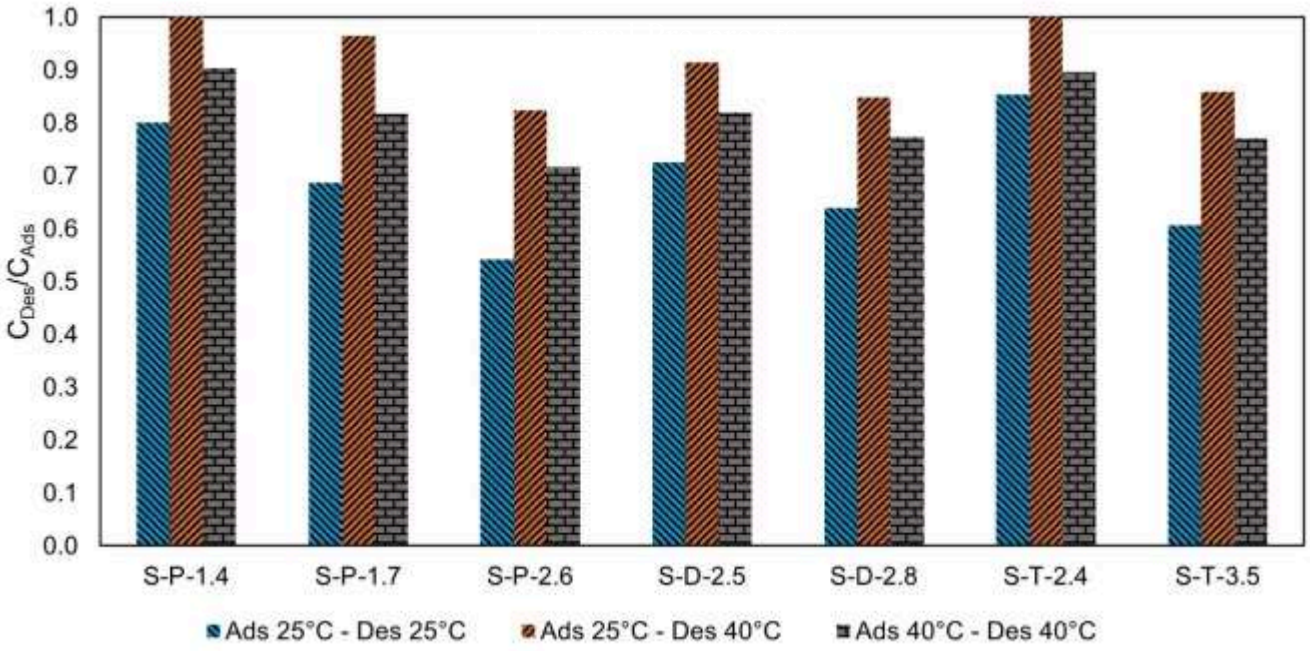

Figure 11. Ratios of desorbed CO_2 per total adsorbed CO_2 (C_{Des}/C_{Ads}) under isothermal and non-isothermal conditions.

In comparison with typical liquid absorbers in amine scrubbing, such as 30wt% MEA and DEA [72], all the grafted samples in this work presented a lower equilibrium capacity. However, MEA 30 wt% was reported to have a heat of adsorption o ~89 kJ/mol, which is higher compared to some of the samples presented here. For example, S-D-2.8's calculated heat of adsorption corresponding to CO_2 loadings above 1.0 mmol/g was ~45 kJ/mol. Similarly, isothermal desorption studies of low-moderate amine loaded SBA-15, such as S-P-1.4 or S-D-2.5, showed a very efficient desorption of CO_2, reported to be between 70 to 90% when purged. Results here summarise the advantages of using sorbents for carbon capture, but a full techno-economic analysis is required for more practical comparison, which draws upon fixed-bed studies of amine functionalised sorbents

4. Conclusions

Different amine types and loadings lead to distinct trends in the adsorption of CO_2 and CH_4, providing key insights on the interactions between the adsorbent surface and adsorbates. The elucidation of the resulting interactions provides necessary information on process and adsorbent design considerations for amine incorporated adsorbents in CO_2/CH_4 separations. In this study, primary amine, diamine, and triamine were grafted on SBA-15 and characterised through structural and chemical morphology by TGA, FTIR, EA, and nitrogen adsorption measurements. It was found that low amine loadings enhanced the adsorption capacity

of CO_2 and its selectivity in CO_2/CH_4 mixtures, while minimising the heat of adsorption associated with chemisorption. Diamine-grafted samples with a moderate surface coverage maintained a low CH_4 adsorption and demonstrated a balance of capture capacity and heat of adsorption that is comparable to high-coverage primary amines. In a similar manner, moderately-grafted primary amine desorbed CO_2 at an efficiency equivalent to densely-grafted primary amines. The variation in amine loading and resulting performance implies that optimal grafting quantities can potentially exist below the maximum surface coverage of an adsorbent base, showing superior uptake and selectivity to CO_2 from CH_4 at atmospheric conditions. They show promise as materials for low pressure processes such as vacuum swing adsorption (VSA). The interaction of CH_4 with amines can be concluded as negligible at around 25-40 °C and 100 kPa, but further studies at higher pressures should be employed to confirm the mode of electrostatic interactions dictating CH_4 adsorption for different amine concentrations. Furthermore, in conventional commercial biogas upgrading by pressure swing processes, the adsorption step occurs at high pressure (>5 bar) to maximise the adsorbed quantity of CO_2. Therefore, exploring the effect of different amines and their functionalities on adsorption at elevated pressure is essential to further advance adsorbents for biogas upgrading, across a wider range of operating processes and conditions.

The presented data indicates that adsorbents with lower amine loadings can balance the distribution of adsorption mechanisms between chemisorption and physisorption, providing an enhancement in adsorbents for the separation of CO_2/CH_4 mixtures while minimising implications on adsorbent regeneration for cyclic applications. Moreover, although moderately amine-grafted sorbents can benefit from higher kinetics and lower heat of adsorption, compared to those that are grafted to maximum loading, their adsorption capacity is lower. Therefore, their cyclic performance for biogas upgrading needs to be further evaluated and optimised using dynamic PSA simulations.

Acknowledgement

The authors would like to thank Howard Smith, Euan Hakon, Jane Hubble, Maria Biskupska, and Richard Andrews for their help and support during the entire experimental work.

Abbreviations

AEAPT	3-(2-aminoethylamino)propyltri-methoxysilane
APS	3-aminopropyltrimethoxysilane
APTES	(3-aminopropyl)triethoxysilane
BdB-FHH	Broekhoff-de Boer - Frenkel-Halsey-Hill
BJH	Barrett-Joyner-Halenda

EA	Elemental analysis
FTIR	Fourier transform infrared spectroscopy
IAST	Ideal gas adsorption solution theory
IR	Infrared
MM	Molecular mechanics
NMR	Nuclear magnetic resonance
PSA	Pressure swing adsorption
PVSA	Pressure vacuum swing adsorption
TAEPT	3-[2-(2-aminoethylamino) ethylamino]propyltrimethoxysilane
TGA	Thermogravimetric analysis
TSA	Temperature swing adsorption
UFF	Universal Forcefield
VSA	Vacuum swing adsorption

Nomenclature

Parameter	Description	Unit
b	Toth isotherm parameter	1/kPa
C_{Des}	Desorption capacity	mmol/g
C_{ads}	Adsorption capacity	mmol/g
D_p	Pore diameter	nm
K	Henry isotherm parameter	mmol/kPa-g
n	Sips isotherm exponent	-
n_s	Toth isotherm parameter	mmol/g
P	Pressure	kPa
Q	Molar uptake	mmol/g
R	Ideal gas constant	J/mol-K
$\hat{S}$	Selectivity	-
S_{BET}	BET surface area	m^2/g
T	Temperature	K
t	Toth isotherm parameter	-
V_p	Pore volume	cm^3/g
ΔH_{Ads}	Isosteric heat of adsorption	J/mol

References

[1] N. Dr. Pieter Tans, scripps institution of oceanography Dr. Ralp Keeling, NOAA/GML, (2021). www.esrl.noaa.gov/gmd/ccgg/trends/ (accessed January 15, 2021).

[2] R.J. Millar, J.S. Fuglestvedt, P. Friedlingstein, J. Rogelj, M.J. Grubb, H.D. Matthews, R.B. Skeie, P.M. Forster, D.J. Frame, M.R. Allen, Emission budgets and pathways consistent with limiting warming to 1.5 °C, Nat. Geosci. 10 (2017) 741–747. https://doi.org/10.1038/ngeo3031.

[3] T.W. (eds. . Masson-Delmotte, V., P. Zhai, H.-O. Pörtner, D. Roberts, J. Skea, P.R. Shukla, A. Pirani, W. Moufouma-Okia, C. Péan, R. Pidcock, S. Connors, J.B.R. Matthews, Y. Chen, X. Zhou, M.I. Gomis, E. Lonnoy, T. Maycock, M. Tignor, IPCC, 2018: Global Warming of 1.5°C., Intergovernmental Panel on Climate Change (IPCC), 2019. https://www.ipcc.ch/site/assets/uploads/sites/2/2019/06/SR15_Full_Report_Low_Res.pdf. (accessed January 7, 2021)

[4] International Energy Agency, World Energy Balances 2019, 2019. https://iea.blob.core.windows.net/assets/8bd626f1-a403-4b14-964f-f8d0f61e0677/World_Energy_Balances_2019_Overview.pdf. (accessed January 12, 2021)

[5] W.M. Budzianowski, K. Postawa, Renewable energy from biogas with reduced carbon dioxide

footprint: Implications of applying different plant configurations and operating pressures, Renew. Sustain. Energy Rev. 68 (2017) 852–868. https://doi.org/https://doi.org/10.1016/j.rser.2016.05.076.

[6] A. Petersson, A. Wellinger, Biogas upgrading technologies-developments and innovations Task 37-Energy from biogas and landfill gas, 2009. www.iea-biogas.net. (accessed July 7, 2020).

[7] A. Golmakani, S.A. Nabavi, V. Manović, Production of negative-emission biomethane by twin double-bed pressure swing adsorption with tail gas sequestration, Chem. Eng. J. 408 (2021) 127312. https://doi.org/https://doi.org/10.1016/j.cej.2020.127312.

[8] D.Y.C. Leung, G. Caramanna, M.M. Maroto-Valer, An overview of current status of carbon dioxide capture and storage technologies, Renew. Sustain. Energy Rev. 39 (2014) 426–443. https://doi.org/10.1016/j.rser.2014.07.093.

[9] A.A. Olajire, CO_2 capture and separation technologies for end-of-pipe applications - A review, Energy. 35 (2010) 2610–2628. https://doi.org/10.1016/j.energy.2010.02.030.

[10] F. Ferella, A. Puca, G. Taglieri, L. Rossi, K. Gallucci, Separation of carbon dioxide for biogas upgrading to biomethane, J. Clean. Prod. 164 (2017) 1205–1218. https://doi.org/10.1016/j.jclepro.2017.07.037.

[11] C.A. Grande, A.E. Rodrigues, Biogas to fuel by vacuum pressure swing adsorption I. Behavior of equilibrium and kinetic-based adsorbents, Ind. Eng. Chem. Res. 46 (2007) 4595–4605. https://doi.org/10.1021/ie061341.

[12] I. Khan, M. Hafiz, D. Othman, H. Hashim, I. Ullah Khan, T. Matsuura, A.F. Ismail, M. Rezaei-Dashtarzhandi, I.W. Azelee, Biogas as a renewable energy fuel – A review of biogas upgrading, utilisation and storage, Energy Convers. Manag. 150 (2017) 277–294. https://doi.org/10.1016/j.enconman.2017.08.035.

[13] L. Pino, C. Italiano, A. Vita, C. Fabiano, V. Recupero, Sorbents with high efficiency for CO_2 capture based on amines-supported carbon for biogas upgrading, J. Environ. Sci. (China). 48 (2016) 138–150. https://doi.org/10.1016/j.jes.2016.01.029.

[14] F. Su, C. Lu, S.-C. Kuo, W. Zeng, Adsorption of CO_2 on amine-functionalized Y-type zeolites, Energy & Fuels. 24 (2010) 1441–1448. https://doi.org/10.1021/ef901077k.

[15] Y. Belmabkhout, R. Serna-Guerrero, A. Sayari, Adsorption of CO_2-Containing Gas Mixtures over Amine-Bearing Pore-Expanded MCM-41 Silica: Application for Gas Purification, Ind. Eng. Chem. Res. 49 (2010) 359–365. https://doi.org/10.1021/ie900837t.

[16] K.A. Fayemiwo, N. Chiarasumran, S.A. Nabavi, K.N. Loponov, V. Manović, B. Benyahia, G.T. Vladisavljević, Eco-Friendly Fabrication of a Highly Selective Amide-Based Polymer for CO_2 Capture, Ind. Eng. Chem. Res. 58 (2019) 18160–18167. https://doi.org/10.1021/acs.iecr.9b02347.

[17] S.A. Nabavi, G.T. Vladisavljević, E.M. Eguagie, B. Li, S. Georgiadou, V. Manović, Production of spherical mesoporous molecularly imprinted polymer particles containing tunable amine decorated nanocavities with CO_2 molecule recognition properties, Chem. Eng. J. 306 (2016) 214–225. https://doi.org/10.1016/j.cej.2016.07.054.

[18] A. Zhao, A. Samanta, P. Sarkar, R. Gupta, Carbon Dioxide Adsorption on Amine-Impregnated Mesoporous SBA-15 Sorbents: Experimental and Kinetics Study, Ind. Eng. Chem. Res. 52 (2013) 6480–6491. https://doi.org/10.1021/ie3030533.

[19] R. Sanz, G. Calleja, A. Arencibia, E.S. Sanz-Pérez, CO_2 capture with pore-expanded MCM-41 silica modified with amino groups by double functionalization, Microporous Mesoporous Mater. 209 (2015) 165–171. https://doi.org/10.1016/j.micromeso.2014.10.045.

[20] X. Xu, C. Song, J.M. Andrésen, B.G. Miller, A.W. Scaroni, Preparation and characterization of novel CO_2 “molecular basket” adsorbents based on polymer-modified mesoporous molecular sieve MCM-41, Microporous Mesoporous Mater. 62 (2003) 29–45. https://doi.org/10.1016/S1387-1811(03)00388-3.

[21] X. Xu, C. Song, J.M. Andresen, B.G. Miller, A.W. Scaroni, Novel Polyethylenimine-Modified

Mesoporous Molecular Sieve of MCM-41 Type as High-Capacity Adsorbent for CO_2 Capture, Energy & Fuels. 16 (2002) 1463–1469. https://doi.org/10.1021/ef020058u.

[22] E.S. Sanz-Pérez, M. Olivares-Marín, A. Arencibia, R. Sanz, G. Calleja, M.M. Maroto-Valer, CO_2 adsorption performance of amino-functionalized SBA-15 under post-combustion conditions, Int. J. Greenh. Gas Control. 17 (2013) 366–375. https://doi.org/https://doi.org/10.1016/j.ijggc.2013.05.011.

[23] A.D. Ebner, M.L. Gray, N.G. Chisholm, Q.T. Black, D.D. Mumford, M.A. Nicholson, J.A. Ritter, Suitability of a solid amine sorbent for CO_2 capture by pressure swing adsorption, Ind. Eng. Chem. Res. 50 (2011) 5634–5641. https://doi.org/10.1021/ie2000709.

[24] N. Hiyoshi, K. Yogo, T. Yashima, Adsorption characteristics of carbon dioxide on organically functionalized SBA-15, Microporous Mesoporous Mater. 84 (2005) 357–365. https://doi.org/10.1016/j.micromeso.2005.06.010.

[25] N. Rao, M. Wang, Z. Shang, Y. Hou, G. Fan, J. Li, CO_2 Adsorption by Amine-Functionalized MCM-41: A Comparison between Impregnation and Grafting Modification Methods, Energy & Fuels. 32 (2018) 670–677. https://doi.org/10.1021/acs.energyfuels.7b02906.

[26] K.C. Vrancken, P. Van der Voort, I. Gillis-d'Hamers, E.F. Vansant, Influence of Water in the reaction of y-Aminopropyltriethoxysilane with Silica Gel, J. Chem. Soc. Faraday Trans. 88 (1992) 3197–3200. https://doi.org/10.1039/FT9928803197.

[27] P. Van Der Voort, I. Gillis-D'Hamers, K.C. Vrancken, E.F. Vansant, Effect of porosity on the distribution and reactivity of hydroxyl groups on the surface of silica gel, J. Chem. Soc. Faraday Trans. 87 (1991) 3899–3905.

[28] E. Vilarrasa-García, J.A. Cecilia, M. Bastos-Neto, C.L. Cavalcante, D.C.S. Azevedo, E. Rodriguez-Castellón, CO_2/CH_4 adsorption separation process using pore expanded mesoporous silicas functionalizated by APTES grafting, Adsorption. 21 (2015) 565–575. https://doi.org/10.1007/s10450-015-9700-x.

[29] L. Wang, R.T. Yang, Increasing selective CO_2 adsorption on amine-grafted SBA-15 by increasing silanol density, J. Phys. Chem. C. 115 (2011) 21264–21272. https://doi.org/10.1021/jp206976d.

[30] P.J.E. Harlick, A. Sayari, Applications of Pore-Expanded Mesoporous Silicas. 3. Triamine Silane Grafting for Enhanced CO_2 Adsorption, Ind. Eng. Chem. Res. 45 (2006) 3248–3255. https://doi.org/10.1021/ie051286p.

[31] Y. Li, N. Sun, L. Li, N. Zhao, F. Xiao, W. Wei, Y. Sun, W. Huang, Grafting of Amines on Ethanol-Extracted SBA-15 for CO_2 Adsorption., Mater. (Basel, Switzerland). 6 (2013) 981–999. https://doi.org/10.3390/ma6030981.

[32] Y. Belmabkhout, A. Sayari, Isothermal versus non-isothermal adsorption-desorption cycling of triamine-grafted pore-expanded MCM-41 mesoporous silica for CO_2 capture from flue gas, Energy and Fuels. 24 (2010) 5273–5280. https://doi.org/10.1021/ef100679e.

[33] M.A. Alkhabbaz, P. Bollini, G.S. Foo, C. Sievers, C.W. Jones, Important Roles of Enthalpic and Entropic Contributions to CO_2Capture from Simulated Flue Gas and Ambient Air Using Mesoporous Silica Grafted Amines, J. Am. Chem. Soc. 136 (2014) 13170–13173. https://doi.org/10.1021/ja507655x.

[34] L. Mafra, S. Schneider, P. V Wiper, R.B. Gomes, L. Pinto, Structure of Chemisorbed CO_2 Species in Amine-Functionalized Mesoporous Silicas Studied by Solid-State NMR and Computer Modeling, J. Am. Chem. Soc. 139 (2017) 389–408. https://doi.org/10.1021/jacs.6b11081.

[35] L. Mafra, T. Čendak, S. Schneider, P. V. Wiper, J. Pires, J.R.B. Gomes, M.L. Pinto, Amine functionalized porous silica for CO_2 /CH_4 separation by adsorption: Which amine and why, Chem. Eng. J. (2018) 612–621. https://doi.org/10.1016/j.cej.2017.12.061.

[36] Y. Belmabkhout, R. Serna-Guerrero, A. Sayari, Adsorption of CO_2 from dry gases on MCM-41 silica at ambient temperature and high pressure. 1: Pure CO_2 adsorption, Chem. Eng. Sci. 64 (2009) 3721–3728. https://doi.org/10.1016/j.ces.2009.03.017.

[37] X. Xu, X. Zhao, L. Sun, X. Liu, Adsorption separation of carbon dioxide, methane and nitrogen on monoethanol amine modified β-zeolite, J. Nat. Gas Chem. 18 (2009) 167–172.

[38] C.-J. Yoo, L.-C. Lee, C.W. Jones, Probing Intramolecular versus Intermolecular CO_2 Adsorption on Amine-Grafted SBA-15, Langmuir. 31 (2015) 13350–13360. https://doi.org/10.1021/acs.langmuir.5b03657.

[39] R. Sanz, G. Calleja, A. Arencibia, E.S. Sanz-Pérez, CO_2 adsorption on branched polyethyleneimine-impregnated mesoporous silica SBA-15, Appl. Surf. Sci. (2010). https://doi.org/10.1016/j.apsusc.2009.12.070.

[40] F. Rouquerol, J. Rouquerol, K. Sing, Adsorption by powders and porous solids., Academic Press, London, 1999.

[41] A. V. Neimark, P.I. Ravikovitch, M. Grün, F. Schüth, K.K. Unger, Pore size analysis of MCM-41 type adsorbents by means of nitrogen and argon adsorption, J. Colloid Interface Sci. 207 (1998) 159–169. https://doi.org/10.1006/jcis.1998.5748.

[42] Lukens Wayne W., P. Schmidt-Winkel, D. Zhao, J. Feng, G.D. Stucky, Evaluating Pore Sizes in Mesoporous Materials: A Simplified Standard Adsorption Method and a Simplified Broekhoff−de Boer Method, Langmuir. 15 (1999) 5403–5409. https://doi.org/10.1021/la990209u.

[43] A.L. Myers, J.M. Prausnit, Thermodynamics of mixed-gas adsorption, AIChE J. 11 (1965) 121. https://doi.org/10.1002/aic.690110125.

[44] K.S. Walton, D.S. Sholl, Predicting multicomponent adsorption: 50 years of the ideal adsorbed solution theory, AIChE J. 61 (2015) 2757–2762.

[45] D.P. Valenzuela, A.L. Myers, O. Talu, I. Zwiebel, Adsorption of gas mixtures: effect of energetic heterogeneity, AIChE J. 34 (1988) 397–402.

[46] M. Thommes, K. Kaneko, A. V Neimark, J.P. Olivier, F. Rodriguez-Reinoso, J. Rouquerol, K.S.W. Sing, Physisorption of gases, with special reference to the evaluation of surface area and pore size distribution (IUPAC Technical Report), Pure Appl. Chem. 87 (2015) 1051–1069. https://doi.org/https://doi.org/10.1515/pac-2014-1117.

[47] N. Hiyoshi, K. Yogo, T. Yashima, Adsorption of carbon dioxide on aminosilane-modified mesoporous silica, J. Japan Pet. Inst. 48 (2005) 29–36. https://doi.org/10.1627/jpi.48.29.

[48] F. Rezaei, M.A. Sakwa-Novak, S. Bali, D.M. Duncanson, C.W. Jones, Shaping amine-based solid CO_2 adsorbents: Effects of pelletization pressure on the physical and chemical properties, Microporous Mesoporous Mater. 204 (2015) 34–42. https://doi.org/10.1016/j.micromeso.2014.10.047.

[49] J. Pires, A. Carvalho, M. Pinto, J. Rocha, Characterization of Y zeolites dealuminated by solid-state reaction with ammonium hexafluorosilicate, J. Porous Mater. 13 (2006) 107–114. https://doi.org/10.1007/s10934-006-7005-x.

[50] T.G. Waddell, D.E. Leyden, M.T. DeBello, The nature of organosilane to silica-surface bonding, J. Am. Chem. Soc. 103 (1981) 5303–5307. https://doi.org/10.1021/ja00408a005.

[51] K.C. Vrancken, P. Van Der Voort, K. Possemiers, E.F. Vansant, Surface and Structural Properties of Silica Gel in the Modification with γ-Aminopropyltriethoxysilane, J. Colloid Interface Sci. 174 (1995) 86–91. https://doi.org/https://doi.org/10.1006/jcis.1995.1367.

[52] R. Serna-Guerrero, Y. Belmabkhout, A. Sayari, Modeling CO_2 adsorption on amine-functionalized mesoporous silica: 1. A semi-empirical equilibrium model, Chem. Eng. J. 161 (2010) 173–181. https://doi.org/https://doi.org/10.1016/j.cej.2010.04.024.

[53] D.D. Do, Adsorption analysis: equilibria and kinetics, Imperial college press London, 1998.

[54] T.W. Swaddle, 6.1.1 Physical Adsorption and Chemisorption, in: Inorg. Chem. - An Ind. Environ. Perspect., Elsevier, 1990: pp. 116–117. https://app.knovel.com/hotlink/pdf/id:kt0099ZFJ4/inorganic-chemistry-an/physical-adsorption-chemisorption BT - Inorganic Chemistry - An Industrial and Environmental Perspective.

[55] J. Friedrich, 3.6 Reaction of Metal Atoms with O-Functional Groups at Polymer Surfaces, in: Met. Syst. - Interface Des. Chem. Bond., John Wiley & Sons, 2018: pp. 95–96. https://app.knovel.com/hotlink/khtml/id:kt011I8T31/metal-polymer-systems/reaction-metal-atoms.

[56] R.J. Littel, G.F. Versteeg, W.P.M. Van Swaaij, Kinetics of CO_2 with primary and secondary amines in aqueous solutions—II. Influence of temperature on zwitterion formation and deprotonation rates, Chem. Eng. Sci. 47 (1992) 2037–2045. https://doi.org/https://doi.org/10.1016/0009-2509(92)80320-C.

[57] F.Y. Chang, K.J. Chao, H.H. Cheng, C.S. Tan, Adsorption of CO_2 onto amine-grafted mesoporous silicas, Sep. Purif. Technol. 70 (2009) 87–95. https://doi.org/10.1016/j.seppur.2009.08.016.

[58] V. Zeleňák, M. Skřínska, A. Zukal, J. Čejka, Carbon dioxide adsorption over amine modified silica: Effect of amine basicity and entropy factor on isosteric heats of adsorption, Chem. Eng. J. 348 (2018) 327–337. https://doi.org/https://doi.org/10.1016/j.cej.2018.04.187.

[59] C.-J. Yoo, S.J. Park, C.W. Jones, CO_2 Adsorption and Oxidative Degradation of Silica-Supported Branched and Linear Aminosilanes, (2020). https://doi.org/10.1021/acs.iecr.9b04205.

[60] A. Sayari, Y. Belmabkhout, E. Da'na, CO_2 Deactivation of Supported Amines: Does the Nature of Amine Matter?, Langmuir. (2012). https://doi.org/10.1021/la204667v.

[61] Y.G. Ko, S.S. Shin, U.S. Choi, Primary, secondary, and tertiary amines for CO_2 capture: Designing for mesoporous CO_2 adsorbents, J. Colloid Interface Sci. (2011). https://doi.org/10.1016/j.jcis.2011.03.045.

[62] T. Čendak, L. Sequeira, M. Sardo, A. Valente, M.L. Pinto, L. Mafra, Detecting Proton Transfer in CO_2 Species Chemisorbed on Amine-Modified Mesoporous Silicas by Using 13C NMR Chemical Shift Anisotropy and Smart Control of Amine Surface Density, Chem. – A Eur. J. 24 (2018) 10136–10145. https://doi.org/https://doi.org/10.1002/chem.201800930.

[63] A.E. Szego, A. Jaworski, N. Hedin, Chemisorption of CO_2 on diaminated silica as bicarbonates and different types of carbamate ammonium ion pairs, Mater. Adv. 2 (2021) 448–454. https://doi.org/10.1039/D0MA00658K.

[64] M.W. Hahn, J. Jelic, E. Berger, K. Reuter, A. Jentys, J.A. Lercher, Role of amine functionality for CO_2 chemisorption on silica, J. Phys. Chem. B. 120 (2016) 1988–1995.

[65] A. Olea, E.S. Sanz-Pérez, A. Arencibia, R. Sanz, G. Calleja, Amino-functionalized pore-expanded SBA-15 for CO_2 adsorption, Adsorption. (2013). https://doi.org/10.1007/s10450-013-9482-y.

[66] S. Choi, J.H. Drese, C.W. Jones, Adsorbent materials for carbon dioxide capture from large anthropogenic point sources, ChemSusChem. 2 (2009) 796–854.

[67] M. V Gil, N. Álvarez-Gutiérrez, M. Martínez, F. Rubiera, C. Pevida, A. Morán, Carbon adsorbents for CO_2 capture from bio-hydrogen and biogas streams: Breakthrough adsorption study, Chem. Eng. J. 269 (2015) 148–158. https://doi.org/https://doi.org/10.1016/j.cej.2015.01.100.

[68] S. Cavenati, C.A. Grande, A.E. Rodrigues, Adsorption Equilibrium of Methane, Carbon Dioxide, and Nitrogen on Zeolite 13X at High Pressures, J. Chem. Eng. Data. 49 (2004) 1095–1101. https://doi.org/10.1021/je0498917.

[69] Z. Bacsik, O. Cheung, P. Vasiliev, N. Hedin, Selective separation of CO_2 and CH_4 for biogas upgrading on zeolite NaKA and SAPO-56, Appl. Energy. 162 (2016) 613–621. https://doi.org/https://doi.org/10.1016/j.apenergy.2015.10.109.

[70] L. Hamon, P.L. Llewellyn, T. Devic, A. Ghoufi, G. Clet, V. Guillerm, G.D. Pirngruber, G. Maurin, C. Serre, G. Driver, W. van Beek, E. Jolimaître, A. Vimont, M. Daturi, G. Férey, Co-adsorption and Separation of CO_2−CH_4 Mixtures in the Highly Flexible MIL-53(Cr) MOF, J. Am. Chem. Soc. 131 (2009) 17490–17499. https://doi.org/10.1021/ja907556q.

[71] L. Bastin, P.S. Bárcia, E.J. Hurtado, J.A.C. Silva, A.E. Rodrigues, B. Chen, A Microporous Metal−Organic Framework for Separation of CO_2/N_2 and CO_2/CH_4 by Fixed-Bed Adsorption, J. Phys. Chem. C. 112 (2008) 1575–1581. https://doi.org/10.1021/jp077618g.

[72] Y.E. Kim, J.A. Lim, S.K. Jeong, Y. Il Yoon, S.T. Bae, S.C. Nam, Comparison of carbon dioxide absorption in aqueous MEA, DEA, TEA, and AMP solutions, Bull. Korean Chem. Soc. 34 (2013) 783–787.

Declaration of interests

☒ The authors declare that they have no known competing financial interests or personal relationships that could have appeared to influence the work reported in this paper.

☐The authors declare the following financial interests/personal relationships which may be considered as potential competing interests:

Highlights:

- Modified SBA-15 by grafting different loadings of primary, di-, and tri-amines
- Desorbate-adsorbent interactions dependent on amine type and loading were studied
- Effect of amine type and coverage on isosteric heat of adsorption was studied
- Isothermal and non-isothermal desorption was evaluated
- Moderate functionalities enhanced CO_2 adsorption and minimised regeneration energy